buildings

Article

Study on Numerical Simulation of Arch Mechanism of Bridge Pile Foundation

Zhanhui Qu [1], Zemin Han [2], Haoyu Tang [2], Jiangbo Xu [2,*], Heping Wang [1] and Yifan Liu [2]

[1] Shaanxi Transportation Holding Group Engineering Technology Co., Ltd., Xi'an 710117, China
[2] School of Highway, Chang'an University, Xi'an 710064, China
* Correspondence: xujiangbo@yeah.net

Abstract: Bridges are situated in a complex area with geological conditions that are challenging for engineering. It has been observed that certain pile foundations of bridges have been uplifted to varying degrees by up to 309 mm. This has a significant impact on the bridge's operation and driving safety. The causal mechanism of the bridge pile foundation arch is analyzed through a theoretical analysis and a Plaxis 3D (v.2013) finite element software simulation. The influence of the ground stress and goaf on the bridge pile foundation under different working conditions is studied. The findings indicate that the uplift of the bridge pile foundation due to an equivalent ground stress is the largest, reaching approximately 300 mm in the bridge valley area. Additionally, the uplift of the non-bridge area in the goaf is greater than that of the bridge pile foundation. These results suggest that ground stress is the primary cause of the arching of a bridge pile foundation.

Keywords: bridge pile arching; Plaxis 3D; ground stress; coal mining airspace; numerical simulation

check for updates

Citation: Qu, Z.; Han, Z.; Tang, H.; Xu, J.; Wang, H.; Liu, Y. Study on Numerical Simulation of Arch Mechanism of Bridge Pile Foundation. *Buildings* **2024**, *14*, 146. https://doi.org/10.3390/buildings14010146

Academic Editor: Weixin Ren

Received: 22 November 2023
Revised: 2 January 2024
Accepted: 4 January 2024
Published: 7 January 2024

1. Introduction

Bridges and tunnels have become the primary means of transportation across mountainous areas due to economic development and technological progress. However, the settlement, arch, and lateral displacement of bridge piers can cause stress redistribution throughout the entire bridge, potentially resulting in irreversible failure. Bridge settlement is a fundamental issue in bridge engineering. Studying the mechanisms behind bridge settlement and foundation uplift can help to understand the causes of pile foundation arch phenomena.

Many scholars have studied the settlement of bridges. Fang, S. et al. [1] studied the influence of existing bridges on the settlement of the piles of nearby bridges. Zhou, T. et al. [2] proposed a method to calculate the long-term settlement of pile foundations which takes into account the consolidation creep characteristics of layered soil at the bottom of the pile. By means of indoor triaxial tests and a finite element numerical simulation, Zhang, C. [3] analyzed the influence of confined water on the settlement of a pile group foundation. Liu, G. [4] analyzed the ground surface of a bridge and the causes of bridge settlement and believed that the subsidence was caused by the collapse of the uncompacted area caused by the influence of rain in the goaf. Liu, J. et al. [5] studied the causes of a settlement disease of the double-pillar pier foundation of a newly built highway bridge and found that an insufficient bearing capacity and pile body defects caused an uneven settlement of the pile foundation. Wang, Y. et al. [6] established the underpass highway model of a high-speed railway bridge by the finite element analysis method and analyzed the settlement between the highway and the bridge. Zhang et al. [7] conducted a numerical simulation study and believed that the shield tunneling technology used in tunnel construction under existing bridges had little influence on the settlement of the existing bridges.

In addition to the research on the mechanism of foundation settlements, scholars at home and abroad have carried out relevant research on the mechanism of foundation uplifts.

Jie, J et al. [8] analyzed a single pile in an expansive soil foundation and obtained the influence of pile length on pile-top uplift under different degrees of expansion. Duan, J. et al. [9] found the uplift characteristics of a trackless subgrade through the water immersion test of an expansive soil foundation. Wang, B. et al. [10] analyzed the deformation of a landslide as the uplift of the front edge of the slope body and obtained the relationship between the temporary confined water and the uplift of the landslide front. Liu, B. et al. [11] collected several engineering cases of the influence of foundation pit excavation on existing underground tunnels and explored the influencing factors of tunnel uplifts and deformations. Zhou, X. et al. [12] conducted a finite element study on the goaf of a coal mine to analyze its uplift mechanism. Krishna, P.H. et al. [13] studied the long-term uplift of expansive soil under different foundations and proposed a foundation treatment method to reduce the uplift. Zhao, J. et al. [14] took a large underground cavern as an example and used the moment tensor multiplication method to clarify the mechanical mechanism controlling the damage mode of the surrounding rock, and revealed the type of cracks in the rock body and the mechanism of the source of the seismic solution. Xu, C. et al. [15] used a new response surface method to assess the risk of goaf uplifts. Biaxial shear tests have been performed on ballasts with different roundness characteristics based on the discrete element method (DEM). The results show that the shear strength slightly increases in the peak state, while a substantial reduction in shear strength is observed in the residual state with increasing roundness [16]. Moreover, an analysis of failure mechanisms has been also conducted in a Stochastic framework [17]. All foundation properties have been investigated in the Stochastic and Machine Learning frameworks [18].

In summary, while there has been extensive research on bridge settlements and foundation uplifts, there remains a dearth of research on bridge pile foundation arches. The research on foundation uplifts may offer some insights for bridge pile foundation arches. This paper analyses the causation mechanism of the pile foundation arch of a bridge through a Plaxis 3D finite element simulation. It also studies the influence of ground stress and gob on the pile foundation arch of the bridge. The findings provide new ideas for bridge pile foundation arches and a reference for bridge deformation treatments.

2. Bridge Area Overview

The bridge is situated in a mountainous area covered with loess and crosses the Ant River at a 30° angle. The bridge pier is affected by bad geological factors such as expansive soil and loess, and there are also coal mined-out areas in the vicinity. The engineering geological environment of the entire bridge is complex. The site of the bridge is covered by sub-sandy soil, loess, and gravel soil on both sides of the riverbed. The channel is covered by pebble soil, beneath which lie strongly weathered sandstone and mudstone, followed by weakly weathered sandstone and mudstone. In 2016, when the relevant units conducted relative elevation measurements of the two bridges, they observed obvious arch phenomena. In 2018, when the absolute elevation was measured, it was found that the two bridges exhibited different degrees of arch phenomena. This was particularly noticeable at the right guardrail of the right half of the #8 pier column of the #1 bridge, where the height changed the most, reaching 309 mm. Table 1 shows the specific data from the field monitoring of the bridge piles (compared to the design elevation).

Table 1. Shiyangtai no. 1 bridge: Dec. 2018 deck lift measurements (mm).

Measurement Point Location		#0	#1	#2	#3	#4	#5	#6	#7	#8	#9	#10
Left	Parapet Side	−5.0	−8.0	0.0	3.0	4.0	18.0	78.0	148.0	295.0	17.0	0.0
	Central Divider Side	−1.0	2.0	3.0	19.0	31.0	51.0	121.0	185.0	258.0	−8.0	−22.0
Right	Parapet Side	−2.0	−3.0	3.0	88.0	112.0	103.0	90.0	267.0	309.0	34.0	−2.0
	Central Divider Side	1.0	−32.0	21.0	97.0	82.0	58.0	51.0	228.0	270.0	−5.0	−21.0

A total of four geological exploration holes were located along the direction of the longitudinal section of the bridge location (at an angle of about thirty degrees with the river). According to the information obtained from the boreholes, the cover layers on both sides of the riverbed at the bridge location are sub-sand, loess, and gravelly soil, and the cover layer of the river channel is pebble soil, which is underneath strongly weathered sandstone and mudstone and then underneath weakly weathered sandstone and mudstone, as shown in Figure 1.

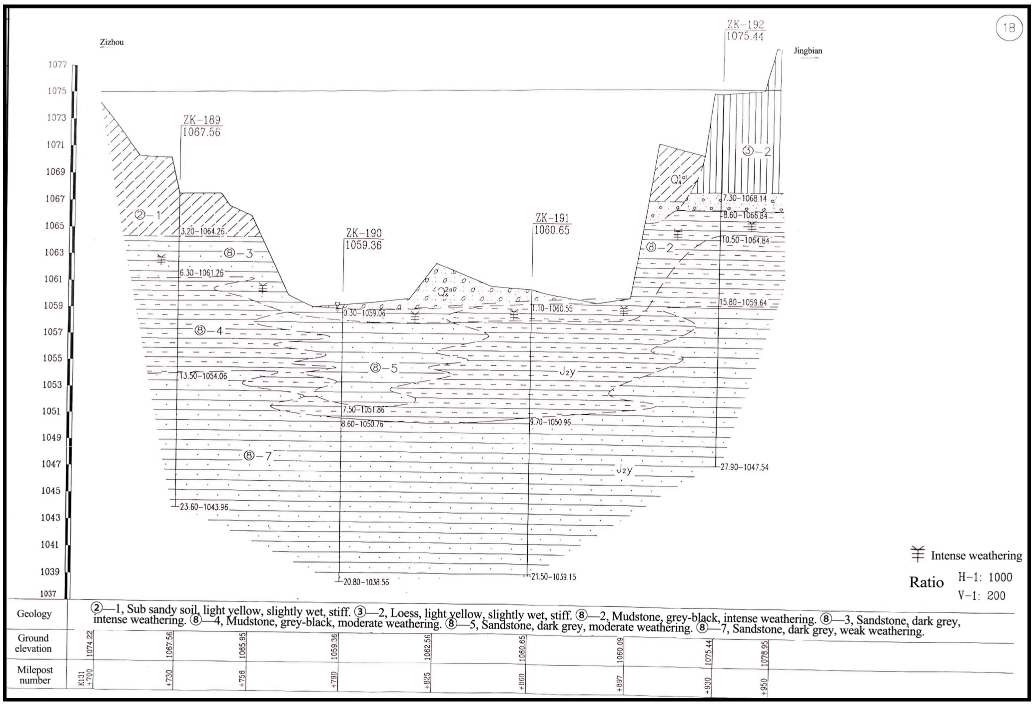

Figure 1. Longitudinal section of the bridge position and geological borehole map.

As can be seen from Figure 2, the east and west sides of the Chinese continental plate are pushed by the Indian Ocean plate and the Pacific plate at a rate of several centimeters per year, while the north and south are constrained by the Siberian plate and the Philippine plate. Under such boundary conditions, the plate mass deforms and produces a horizontal compressive stress field [19]. The bridge is located in the northern Shaanxi Province, which is also the area through which the principal stress trace in the figure crosses, so it can be judged that the bridge is indeed in a high ground stress environment.

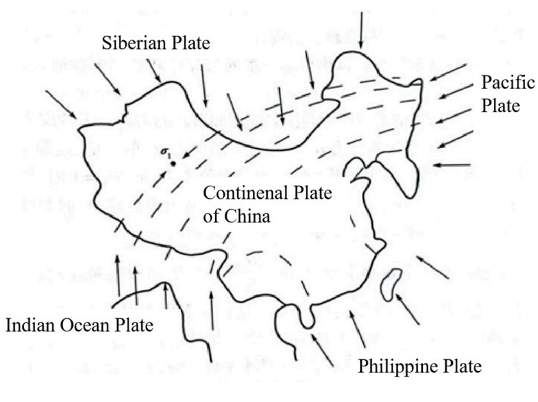

Figure 2. Principal stress trace diagram of China's continental plate.

3. Model Building

Plaxis 3D is a computer program that uses a finite element analysis to evaluate deformations, stability, and permeability in geotechnical engineering. The software boasts a user-friendly interface and easy-to-use operations, with powerful graphical modeling and analysis capabilities. It includes a variety of advanced constitutive relations and can simulate multi-stage construction processes under complex conditions, such as seepage.

The Plaxis 3D modeling process consists of four steps: defining soil and structural unit parameters and meshing, defining boundary and seepage conditions, and executing commands. The modeling process is shown in Figure 3.

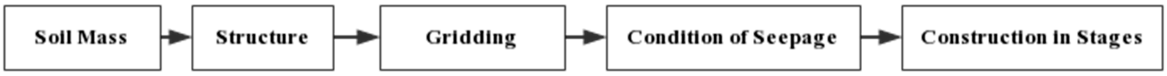

Figure 3. Flow chart of Plaxis 3D software modeling.

3.1. Geological Model

Based on the geological plan and observations, the bridge is situated between two mountains at an angle of approximately 30 degrees to the direction of the river. The two mountains that affect the bridge are located to the northwest and southeast. To account for a wide range of geological conditions, the model is set to 300 m × 300 m with default settings for the rest. The method of drilling data and prediction defined a total of 104 boreholes. Each borehole's formation data and water head data were defined to automatically interpolate and generate the nearest soil layer data, resulting in the establishment of a soil model. Figure 4 displays the borehole location map and the engineering geological model generated from the borehole.

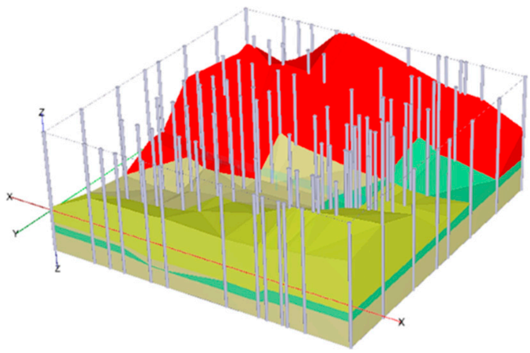

Figure 4. Engineering geological model. Different colors represent strata with different lithologies, for example, red for ③-2 loess, yellow for ⑧-3 sandstone, green for ⑧-4 mudstone, brownish-yellow for ⑧-7 sandstone, and blue for the bridges.

Figure 5 shows the simplified bridge model, which is represented by a solid plate measuring 12 m × 1 m and includes two abutments and nine piers. The piers are numbered from left to right as abutments No. 1 and No. 2 and piers No. 1–9. The largest longitudinal displacement occurs at pier No. 8.

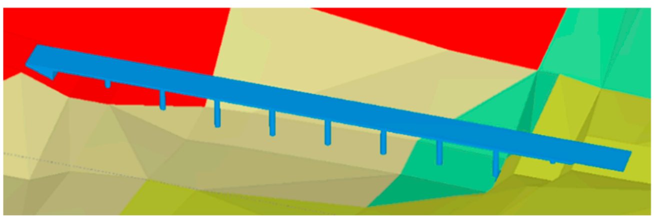

Figure 5. Simplified model of the right half of the bridge.

3.2. Material Characteristics and Boundary Conditions

The material is classified as mudstone, following the Mohr–Coulomb criteria. The main materials of the bridge pile foundation are rebar and concrete, which exhibit characteristics of a linear elastic structure. Therefore, the bridge facilities are classified as a linear elastic structure. Table 2 defines the characteristics of the mudstone based on the engineering geological report of the bridge location.

Table 2. Characteristics of mudstone materials.

Project	Parameter Values
Nature Density $\gamma/(\text{kN/m}^3)$	24.18
Saturated Density $\gamma_{sat}/(\text{kN/m}^3)$	24.35
Void Ratio e	0.02
Modulus of Elasticity $E/(\text{kN/m}^2)$	4.11×10^5
Poisson Ratio ν	0.232
Cohesive Strength $c/(\text{kN/m}^2)$	112.6
Internal Friction Angle $\Phi/(°)$	26

The model assumes normal fixed conditions for all aspects except for the z-axis max direction. By default, the z-axis min direction is set to completely fixed. This can remain unchanged as the displacement boundary condition of the ground stress is forced to apply and the boundary deformation condition of Z_{min} does not affect the application of the ground stress, as shown in Figure 6.

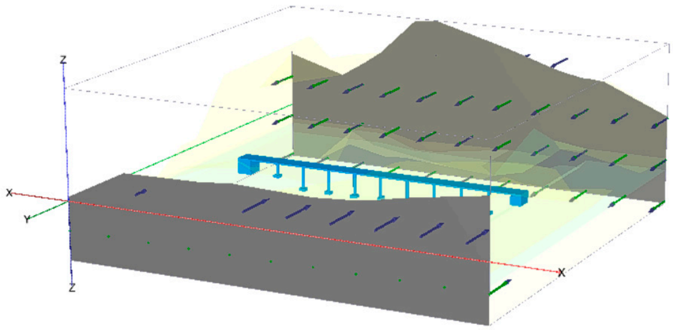

Figure 6. The case of applying displacement boundary conditions.

Figure 6 shows that ground stresses are applied to the boundary from the y-axis (i.e., north–south direction). Ground stress can be categorized into load and displacement forms. The software locks the displacement of the underlying soil when the load is applied, resulting in the ground stress being applied in the form of displacement.

3.3. Goaf Model

In 2001, Zhang, Z [20] conducted a study on the uplift mechanism of the Hancheng Power Plant. They proposed a new understanding of why large areas of goafs experience direct roof collapses. The sand-covered mudstone layer in the collapse zone becomes a composite slab beam that bears a huge overburden. The subsidence bending deformation of the slab beam is accompanied by interlayer dislocations between the sand–mudstone layers, which develops towards the front of the mountain. This expansion of the separation layer and rock mass produces a lateral pushing effect on the underlying bedrock of the plant, causing the peristaltic deformation of upward bending and uplifts of the near-horizontal sand–mudstone layer under the foundation of the plant. This expansion of the separation layer and rock mass produces a lateral pushing effect on the underlying bedrock of the plant, causing peristaltic deformation of upward bending and uplifts of the near-horizontal sand–mudstone layer under the foundation of the plant. This is an epigenetic aging deformation caused by underground mining.

To determine the validity of this theory in the engineering geological environment of the bridge, it is necessary to model the gob around the bridge site. This theory requires a certain pressure from the soil above the goaf; therefore, it is more reasonable to construct the goaf under the mountain.

Figure 7 shows the geometry model of the goaf. Once the goaf contour is established, the plane is stretched to 120 m and embedded into the mountain in the southeast of the bridge. The gob area will be excavated here, so no materials need to be set up. Additionally, ground stress does not need to be considered under these conditions.

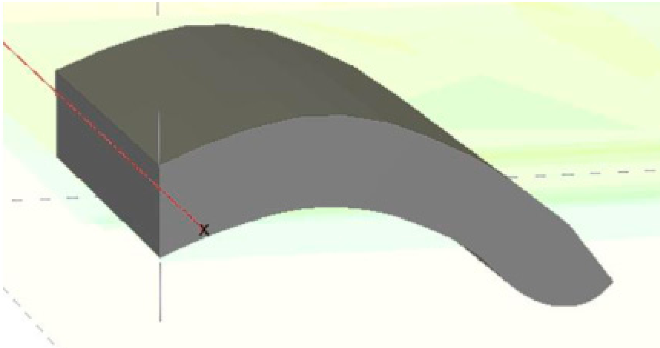

Figure 7. Geometric model of goaf.

Figure 8 shows the grid division diagram of the goaf model. The grid generator requires the global density parameter to determine the cell mesh size (l_e). In Plaxis 3D, this is calculated from the external geometry (x_{min}, x_{max}, y_{min}, y_{max}, z_{min}, z_{max}), and the cell density is selected from the Cell Distribution drop-down menu in the Grid Options window. The formula for calculating the cell mesh size is as follows:

$$l_e = \frac{r_e}{20}\sqrt{(x_{max} - x_{min})^2 + (y_{max} - y_{min})^2 + (z_{max} - z_{min})^2} \quad (1)$$

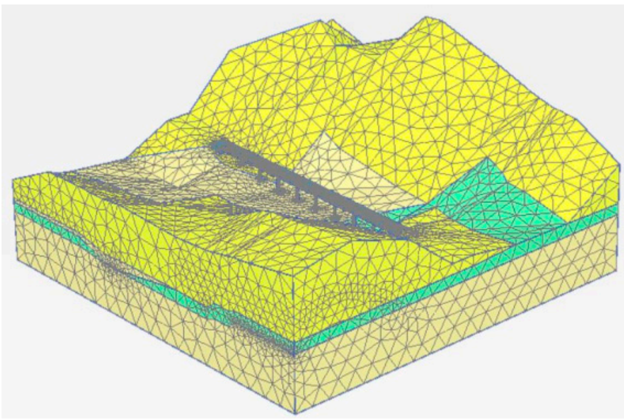

Figure 8. Grid division diagram of goaf model.

In the formula, r_e is the relative unit size factor, which is used to represent the global thinning density. The values are taken according to Table 3:

Table 3. Different global density levels r_e.

Global Density Level	Value r_e
Very Coarse	2.0
Coarse	1.5
Medium	1.0
Fine	0.7
Very Fine	0.5

4. Numerical Simulation Results and Analysis

4.1. Numerical Simulation of Ground Stress

Based on the analysis of geological data and models, it is estimated that the height difference between the two mountains and the bottom of the valley near the bridge site is almost 90 m. It is hypothesized that the mountain will exert a compressive force on the soil beneath the bridge due to its own weight, leading to the arching of the foundation soil and subsequent lifting of the pier column.

To achieve the purpose of a comparative test, the Plaxis 3D (2013) software was used to conduct a multi-condition modeling analysis of the bridge and its engineering geological environment. And the displacement data in the z-axis direction was obtained. The rock layer, with a depth of about 40 m, was measured. Based on the actual situation, it is divided into the following four conditions to simulate the influence of ground stress on the bridge pile foundation.

(1) The first working condition is the natural bridge state without any applied ground stress.

(2) The second working condition is the bridge state with an equivalent ground stress applied.

(3) The third working condition is the bridge state with the ground stress distributed along the Z-axis.

(4) The fourth working condition is a simplified model of the second pier column of the bridge, where an equivalent ground stress is applied, and the bridge pressure on the pier column is simplified into a uniform load distributed at the top of the pier.

By analyzing conditions 1 and 2, the difference of the pier arch condition between the natural state and the high ground stress state can be obtained. Comparing working conditions 2 and 3 allows us to compare two different ground stress states and to identify which condition has the greatest influence on the results. The results can be verified by comparing working conditions 2 and 4. If the difference is too large, the results are incorrect.

4.1.1. Working Condition 1: Natural Bridge-Formation State without Applying Ground Stress

This condition represents the intermediate state of any given condition, which can be observed in the output results. Figure 9 displays the z-axis displacement diagram during the construction phase of the 'Completed Bridge'. Figure 10 shows the z-axis displacement diagram of the section where the center line of the bridge floor is located.

The displacement diagram of the bridge state above shows that the bridge position has a relatively small displacement, controlled between ±20 mm. Settlement has occurred in almost all piers, with a range of about 10~20 mm. The observed displacement of 309 mm is significantly large. This discrepancy suggests that the initial hypothesis—that the gravitational force of the two mountains compresses the soil beneath the bridge, causing the foundation soil to form an arch and subsequently lifting the pier column, leading to changes in the bridge's linearity—is likely incorrect.

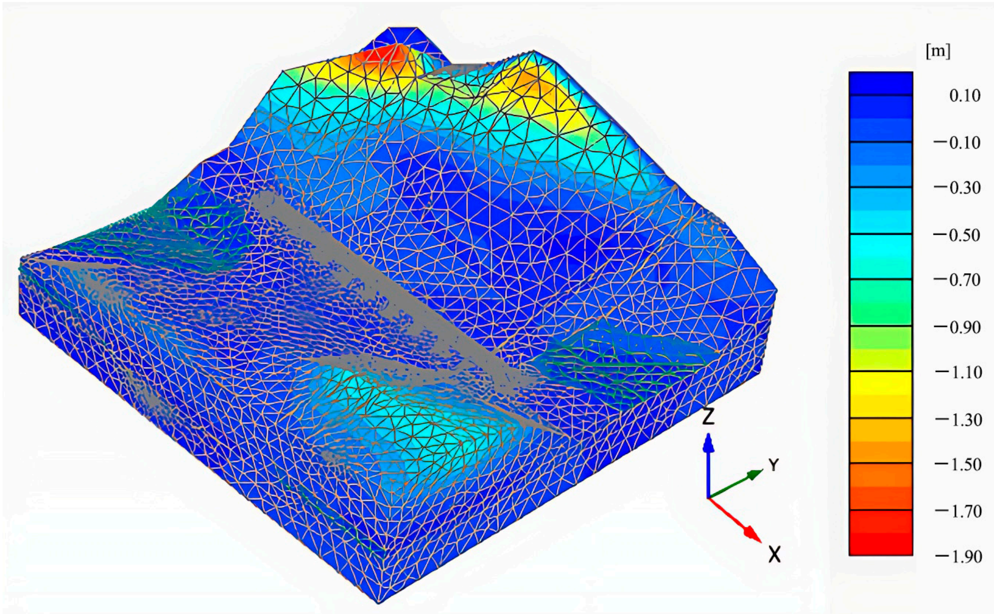

Figure 9. Z-axis displacement map during the "Bridge Construction" stage.

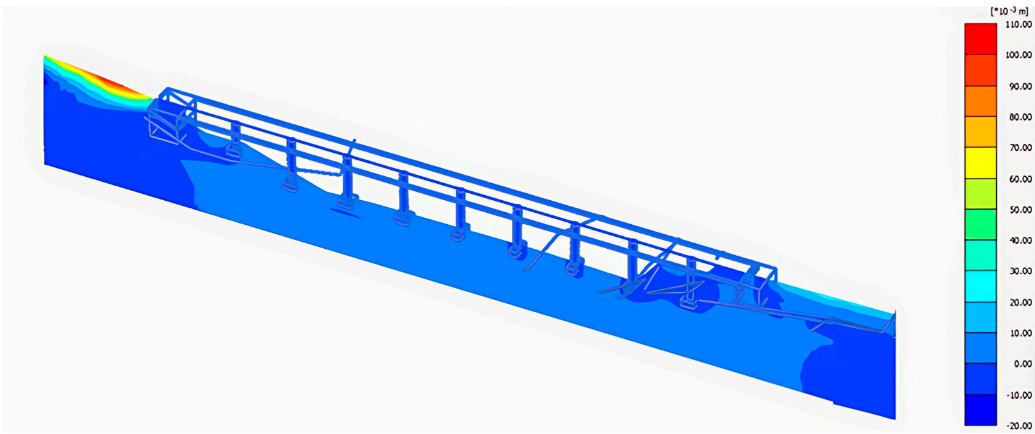

Figure 10. Z-axis displacement of the centerline of the bridge deck.

4.1.2. Working Condition 2: The Bridge-Formation State with Equivalent Ground Stress Applied

The displacement boundary condition is chosen as the ground stress, with a displacement value of 0.5 m applied to the interface of *Ymin* and *Ymax* simultaneously. This ensures that the normal displacement is perpendicular to the bridge. The total strain value in the Y direction is $\varepsilon = 1/300$. Based on the elastic modulus of the sandstone, which is $E = 3.4 \times 10^3$ MPa, the calculation can be performed as follows (Hast, 1970s):

$$\sigma = \varepsilon \cdot E = \frac{1}{300} \times 3.4 \times 10^3 = 11.33 \text{ MPa} \tag{2}$$

Upon reviewing the horizontal ground stress table of Scandinavia, Finland published by Hast in the 1970s, it is evident that there are 13 locations where the measuring point is approximately 60 m or less below the surface, and the horizontal principal ground stress of the rock strata can exceed 10 MPa. Thus, in regions with a high ground stress, the horizontal principal earth stress of the rock layer at a depth of about 60 m can surpass 20 MPa.

After calculating the value of the applied ground stress, it is adjusted to the calculation stage and then applied to the model, as illustrated in Figure 11.

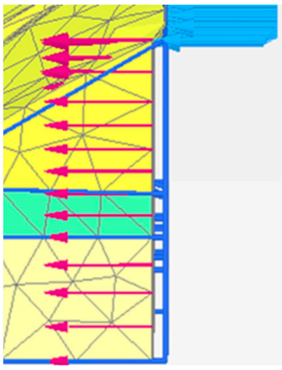

Figure 11. Distribution of ground stress (displacement).

The fixed boundary condition of the bottom surface of the Z-axis causes the rock mass to arch upward under the action of ground stress, which results in the pile foundation of the bridge to lift and causes linear changes to the bridge.

Figure 12 shows that the foundation soil in the valley has been raised to varying degrees, approximately 300 mm. The influence of the dead weight of the mountain on both sides on the soil lifting has been excluded in the working condition. Therefore, it can be concluded that the lifting of the valley under this working condition is mainly caused by ground stress.

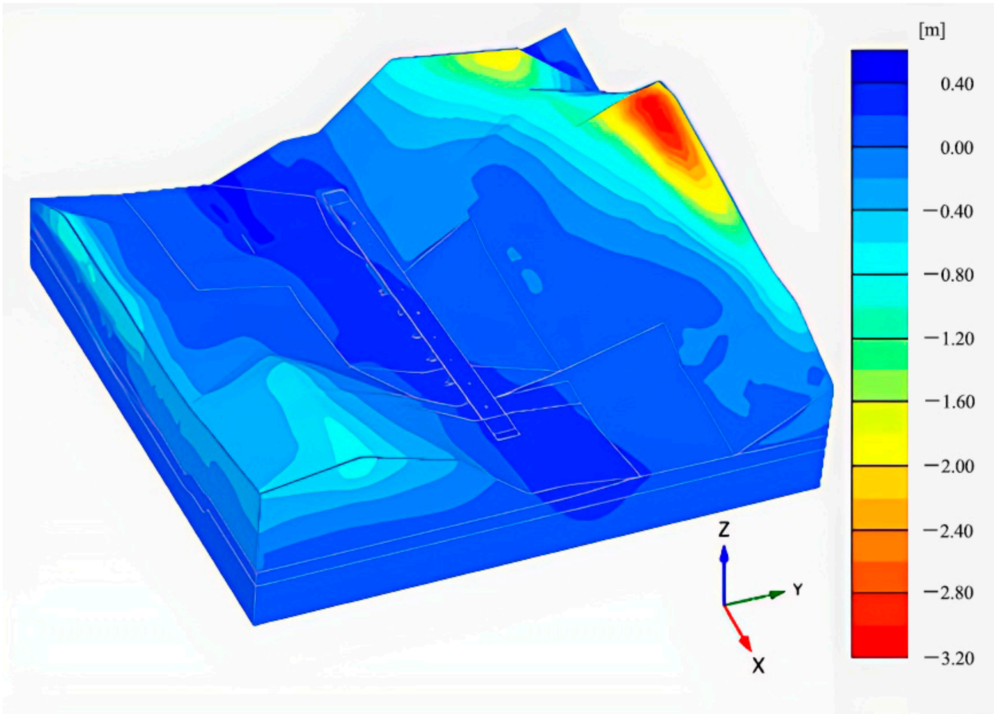

Figure 12. The z-axis direction displacement underground stress.

The measured results indicate that the upper arch value of the first pier is smaller, while the upper arch value of the second pier is larger, which is consistent with the uplift of the pier shown in Figure 13.

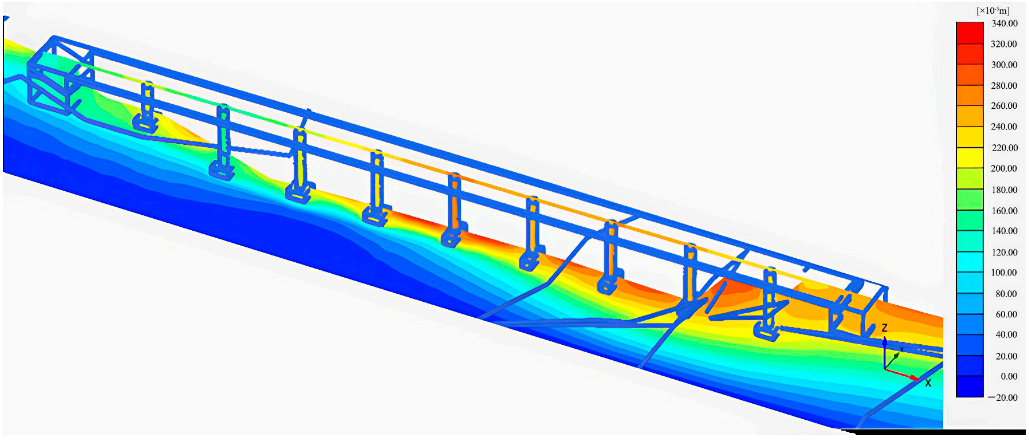

Figure 13. The z-axis displacement diagram of the section at the center line of the bridge deck.

The analysis focuses on the lifting of the second pier, which is approximately 260 mm, consistent with the measured value. For instance, the uplift measured at the guardrail of pier #7 was 267 mm, and at the measured guardrail of pier #8, it was 309 mm. Considering the expansion of the expanding rock, this working condition can be deemed a successful simulation of the actual situation.

4.1.3. Working Condition 3: Bridge-Formation State of Ground Stress Harmoniously Distributed along the Z-Axis Direction

Plan 1: The ground stress increases gradually from 40 m underground. The displacement value is set to 0, resulting in a change value of 0.025 m/m. This indicates a horizontal displacement value of 0.025 m per meter on the z-axis.

The upper layer of sandstone is mudstone, which has an elastic modulus one order of magnitude lower than that of sandstone. The upper layer is loess, which has an elastic modulus two orders of magnitude lower than that of mudstone. Therefore, only the sandstone layer is considered when estimating the ground stress level. Currently, the maximum displacement of the sandstone layer is only 0.4 m. Following the calculation method in working condition 2, the maximum ground stress is calculated as follows:

$$\sigma = \varepsilon \cdot E = \frac{0.4 \times 2}{300} \times 3.4 \times 10^3 = 9.07 \text{ MPa} \tag{3}$$

According to the study in the second condition, 9.07 MPa is the ground stress value that can be generated completely.

As can be seen from Figures 14 and 15, although there is lift in the valley under this condition, it is not obvious. The lift at the bridge section is also concentrated in the first connection, not the second connection.

Plan 2 outlines that the ground stress decreases gradually from 40 m underground, with a displacement value of 1 m. The z-axis coordinate of the highest point is 0 m, with a displacement value of 0. Therefore, the change value is set to -0.025 m/m (the negative sign indicates the negative direction of the y-axis). This means that there is a horizontal displacement value of 0.025 m per meter change on the z-axis.

The maximum horizontal ground stress is calculated based on the displacement value of the sandstone. In this case, the maximum displacement of the sandstone is 1 m, and the maximum ground stress can be estimated as follows:

$$\sigma = \varepsilon \times E = (1 \times 2)/300 \times 3.4 \times 10^3 = 22.67 \text{ MPa} \tag{4}$$

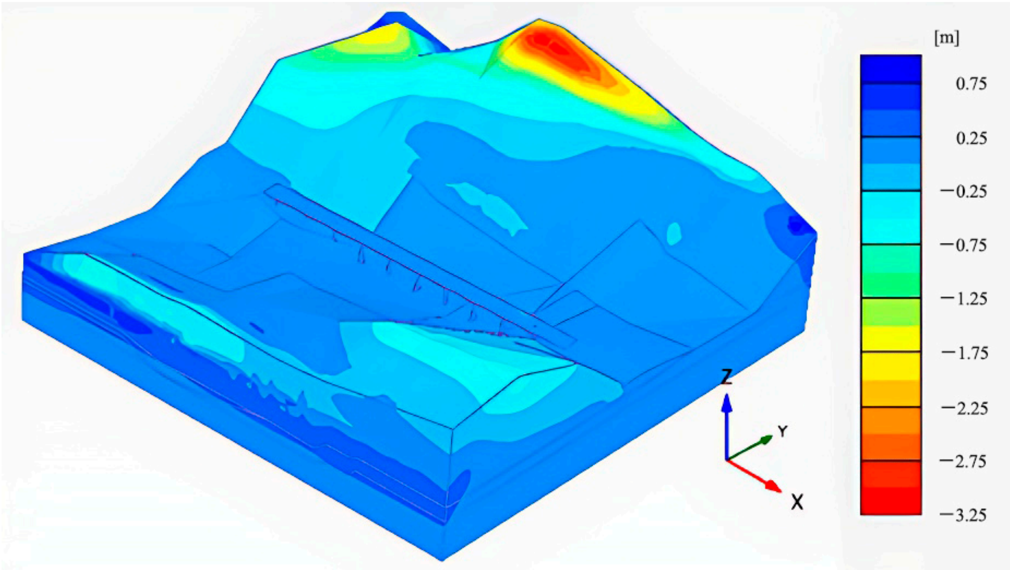

Figure 14. Displacement of the z-axis direction along the z-axis.

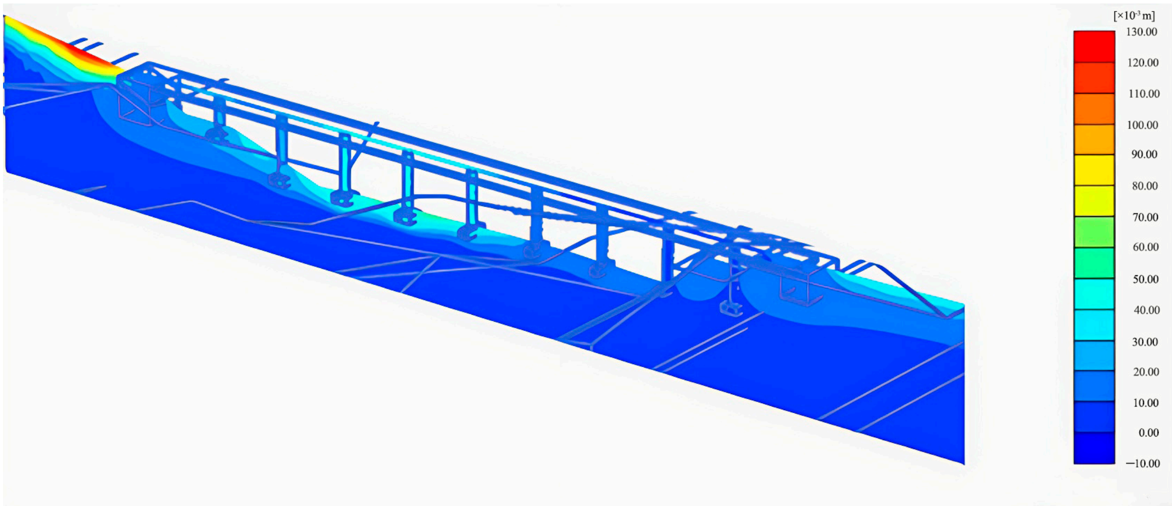

Figure 15. The z-axis displacement diagram of the section at the center line of the bridge deck.

Figures 16 and 17 clearly show an uplift at the valley, while the displacement at the second joint of the bridge can reach up to 340 mm, which exceeds the actual situation. Plan 2 is closer to the actual situation than Plan 1, despite having the same displacement change mode and average displacement. This is in line with the results of condition 2.

Compared to condition 2, the ground stress model used in Plan 2 of condition 3 provides a more accurate simulation of the actual situation. Specifically, the ground stress increases with depth. According to the comparative study of working conditions 2 and 3, it can be concluded that the contribution of displacement caused by shallow ground stress to the foundation arch is relatively low within a certain depth from the ground. Conversely, the foundation arch caused by deep ground stress is much larger.

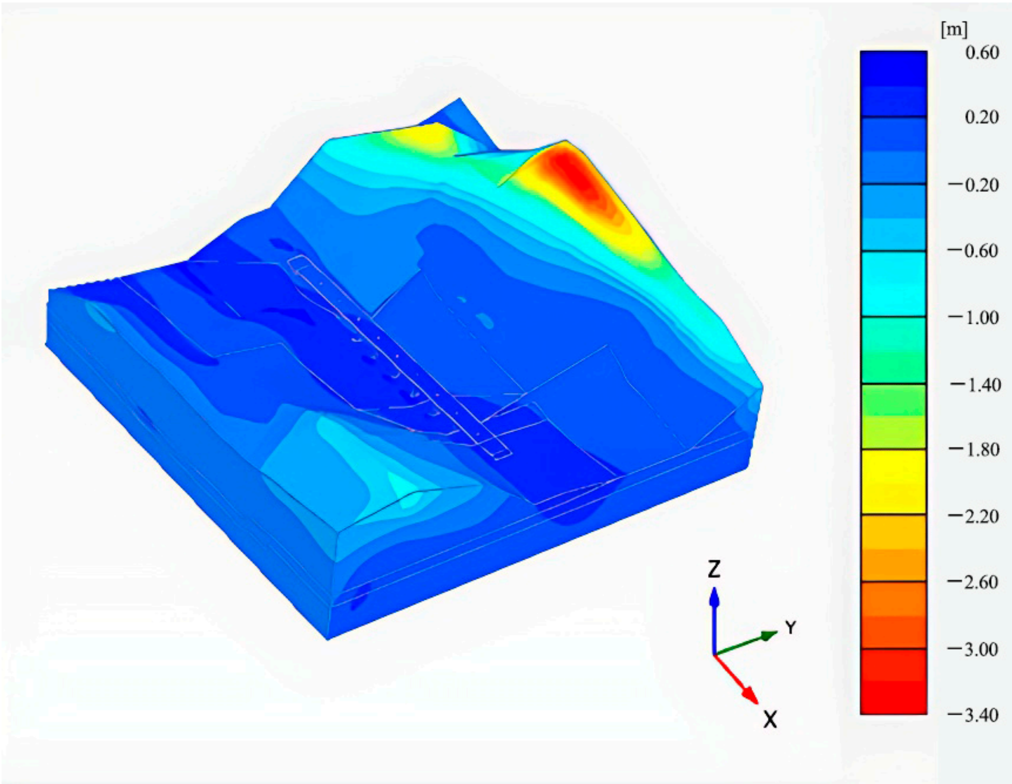

Figure 16. Displacement of the z-axis direction along the z-axis.

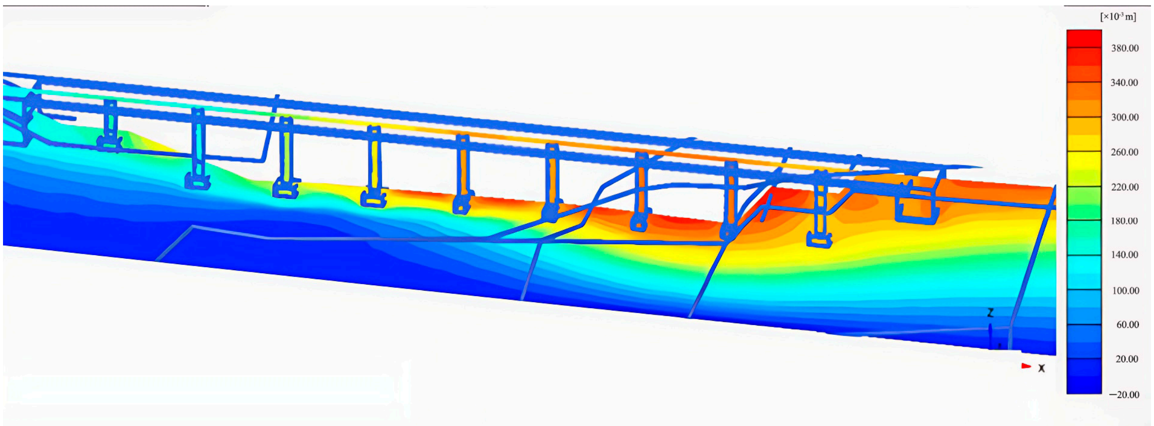

Figure 17. The z-axis displacement diagram of the section at the center line of the bridge deck.

4.1.4. Working Condition 4: The Simplified Model of the Second Joint Pier Column of the Bridge

In this working condition, the bridge is modeled as a simplified pier column, and the bridge pressure on the pier columns is represented as a uniform load distributed at the top of the pier. Only an equivalent ground stress is applied in the y-axis direction, as in the second working condition. This working condition is used solely to verify the results of the second working condition.

The top reaction forces of the piers in the completed bridge state are 1296.4 kN, 3618 kN, 3146.4 kN, 3146.4 kN, and 3618 kN, respectively. Specifically distributed to each pier top of the uniform load are 412.9 kN/m^2, 1152 kN/m^2, 1001 kN/m^2, 1001 kN/m^2, and 1152 kN/m^2.

The z-axis displacement distribution of working condition 4 is similar to that of working condition 2 in Figure 18, with only a slight difference in value. This difference is acceptable since the reaction force of the pier top under the design load during bridge construction is used, rather than the data from several years of actual use. Thus, condition 4 confirms the simulation of condition 2.

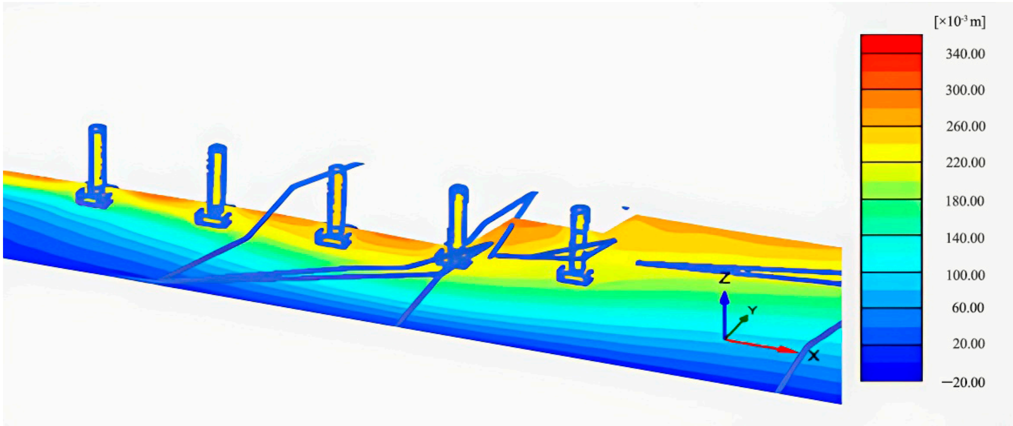

Figure 18. The z-axis displacement diagram of the section at the center line of the bridge deck.

4.2. Numerical Simulation of the Goaf Area

This paper examines the formation and collapse of the goaf through a simplified model, using a specific case study. The depth of the goaf is limited to 40–60 m, causing it to arch along the mountain. The length of the goaf is set at 120 m, covering pier No. 7, 8, and 9 of the bridge pile foundation, as well as the right abutment. Furthermore, the height difference between the highest and lowest points of the goaf is approximately 20 m. The goaf extends towards the bridge direction for around 100 m and is approximately 50 m away from the bridge's center line.

The numerical simulation of the goaf considers two types of working conditions: (1) the influence of the goaf on the valley area under natural conditions, and (2) the influence of the goaf on the valley area under bridge conditions.

4.2.1. Working Condition 1: Impact of Goaf on River Valley Area under Natural State

In the natural state, without the local bridge being built, we can obtain data for the control group by simulating the influence of the caving arch of the goaf on the valley area.

As shown in Figure 19, the arch on the left side of the figure is only within the range of 0–10 mm, while the arch on the right side is more pronounced, reaching up to 160 mm. The piers are almost non-existent where they should have been. The arch in the original abutment location measures approximately 40 mm. However, the arch on the foundation is evident in the soil outside the bridge's range.

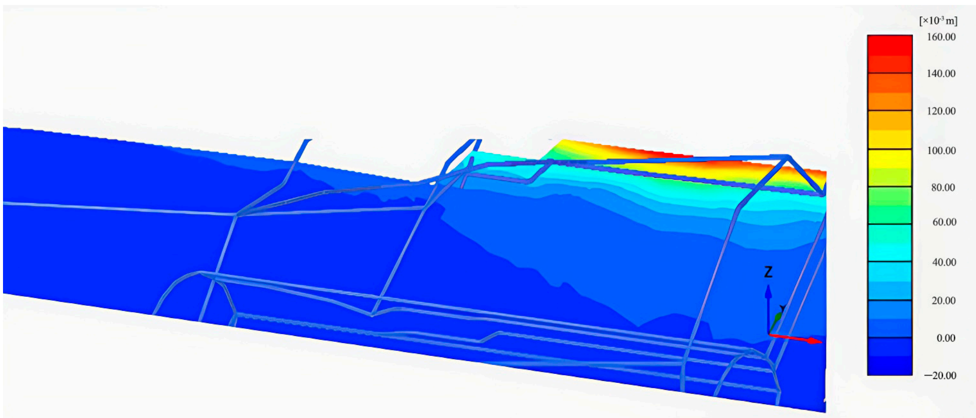

Figure 19. Z-axis displacement diagram of the bridge center line interface in the 'goaf' phase.

4.2.2. Working Condition 2: Impact of Goaf on River Valley Area under Bridge-Formation State

Figures 20 and 21 demonstrate that the soil in the upper part of the goaf has settled, and the soil at the arch foot of the collapse arch has risen. Compared to the results in Figures 18 and 20, the z-axis displacement in the area with piers decreased slightly in this working condition. The maximum lift of the abutment area decreased by about 30 mm, which is only about 100 mm. In the non-bridge structure area, the maximum vertical displacement increased to 198 mm.

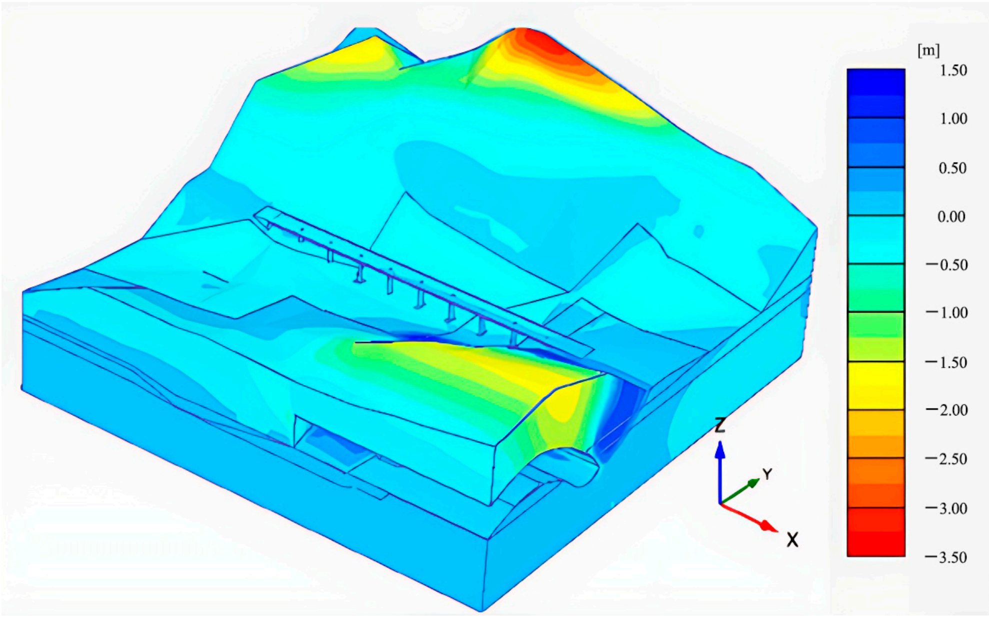

Figure 20. The z-axis displacement diagram in the goaf stage.

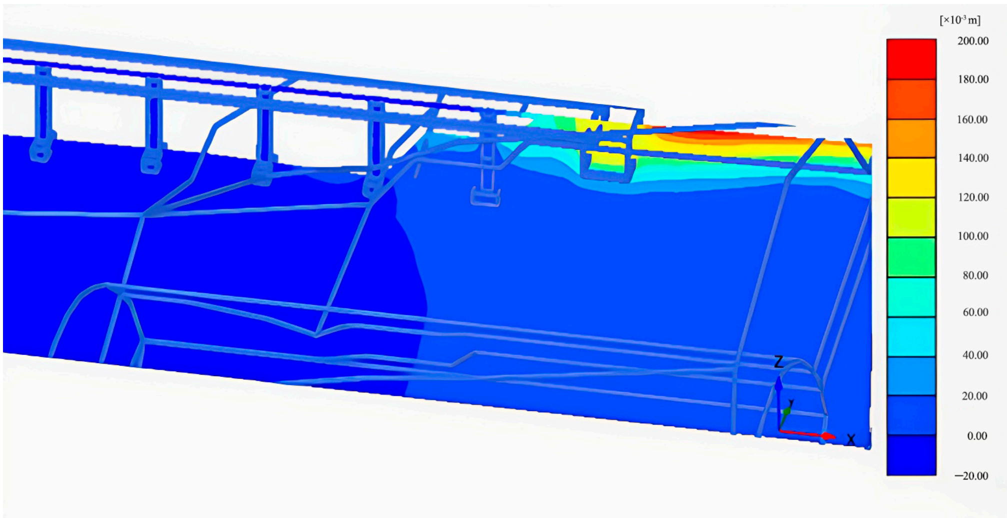

Figure 21. Z-axis displacement diagram of the bridge center line interface in the "goaf" phase.

5. Conclusions

This study investigated the impact of ground stress and gob on bridge pile foundations using a Plaxis 3D numerical simulation. The main causal mechanism of bridge pile foundation arches was determined. The specific conclusions are as follows:

(1) Bridge piers in the valley area will experience varying degrees of uplifts under different forms of ground stresses. When subjected to an equivalent ground stress, the

pier lifts a maximum of 300 mm, which is in line with the measured value of 309 mm. The maximum lifting position of the pier is also consistent with reality. Although the maximum lifting position of the bridge pier is the same, it lifts to a height of 340 mm, which is greater than the measured value.

(2) The goaf provides resistance to the uplift of bridge piers in the valley area. The maximum uplift of bridge piers in the area with a goaf is approximately 100 mm, which is lower than that in the area without a goaf. The lifting rules for each region, including the goaf, are as follows: soil lifting in the non-bridge structure region > soil lifting in the abutment region > soil lifting in the pier region.

(3) Upon comparing the numerical simulation results under the ground stress conditions with the field monitoring values, it is evident that the numerical simulation results are consistent with the measured values. Thus, it can be concluded that the upward arch of the bridge pile foundation is primarily caused by ground stress.

Author Contributions: Writing-original draft, Z.Q.; Formal analysis, Z.H.; Methodology, H.T.; Conceptualization, J.X.; Funding acquisition, H.W.; Writing-review & editing and Software, Y.L. All authors have read and agreed to the published version of the manuscript. For the record, the research paper presented is the result of the joint efforts of all listed authors. Except for those already cited in the text, this paper does not contain the results of any other individual or collective published or written works. Individuals and collectives who have made significant contributions to the research work of this paper have been identified as authors in the text.

Funding: This research was funded by the China Natural Science Foundation under Grant No. 42007254, the Science and Technology Plan Project of Housing and Urban-Rural Construction in Shaanxi Province (2022-K53), Innovation Capability Support Program of Shaanxi (Program No. 2023-CX-TD-35) and Key Research and Development Program of Shaanxi (Program No. 2023KXJ-159).

Data Availability Statement: The data used to support the findings of this study are available from the corresponding author upon request. The data are not publicly available due to privacy.

Conflicts of Interest: Authors Zhanhui Qu and Heping Wang were employed by the company Shaanxi Transportation Holding Group Engineering Technology Co., Ltd. The remaining authors declare that the research was conducted in the absence of any commercial or financial relationships that could be construed as a potential conflict of interest.

Notation

l_e	cell mesh size
r_e	relative unit size factor
x_{max}	maximum size of the model in the x-axis direction
x_{min}	minimum size of the model in the x-axis direction
y_{max}	maximum size of the model in the y-axis direction
y_{min}	minimum size of the model in the y-axis direction
z_{max}	maximum size of the model in the z-axis direction
z_{min}	minimum size of the model in the z-axis direction
E	the elastic modulus of sandstone
ε	total strain value
σ	maximum ground stress value

References

1. Fang, S.; Xu, X.; Wang, T. Influence of New Bridge Loading on Additional Foundation Settlement of Existing Bridge. *J. Railw. Sci. Eng.* **2022**, *19*, 1187–1195.
2. Zhou, T.; Xu, F.; Yang, Q.; Wu, Y. A Method for Calculating the Consolidation and Creep-induced Settlement of Bridge Pile Foundation of High-speed Railway. *J. Railw. Sci. Eng.* **2021**, *18*, 1968–1977.
3. Zhang, C.; Zhao, Y.; Zhang, Z.; Zhu, B. Case Study of Underground Shield Tunnels in Interchange Piles Foundation Underpinning Construction. *Appl. Sci.* **2021**, *11*, 1611. [CrossRef]
4. Liu, G. Reasons Analysis and Treatment of Foundation Subsidence in Bridge Later Period under Mining Influence. *J. Min. Strat. Control Eng.* **2019**, *24*, 86–89+119.

5. Liu, J. Evaluation Analysis and Reinforcement Treatment for Settlement of Double-column-type Highway Bridge Pier Foundation. *Railw. Eng.* **2018**, *58*, 27–29+41.
6. Wang, Y.; Liang, S.; Huang, C.; Wang, R. Foundation Settlement Response of Existing High-Speed Railway Bridge Induced by Construction of Undercrossing Roads. *Sustainability* **2022**, *14*, 8700. [CrossRef]
7. Zhang, C. Analysis of Settlement Characteristics of Friction Pile Groups of High Speed Railway Bridge Caused by Pressure Drop of Confined Water. *Railw. Eng.* **2021**, *61*, 36–40.
8. Jie, J.; Hou, K.; Ou, X.; Liu, Z.; Long, T. Nonlinear Analysis of Bearing Characteristics of Single Pile in Expansive Soil. *J. Basic Sci. Eng.* **2021**, *29*, 741–751.
9. Duan, J.; Yang, G.; Liu, Y.; Kan, J.; Qiu, M. Deformation characteristics of double-line ballastless track subgrade under water immersion of expansive rock foundation. *J. Cent. South Univ. Sci. Technol.* **2020**, *51*, 156–164.
10. Wang, B.; Xu, B.; Liu, H. Failure Model Analysis for Piedmont Gentle Slopes Due to Temporary Confined Water. *Geol. J. China Univ.* **2020**, *26*, 665–673.
11. Liu, B.; Zhang, D.; Yang, W.; Li, X. Prediction formula and its application of underlying existing tunnel heave induced by deep excavation based on case statistics. *J. Cent. South Univ. Sci. Technol.* **2022**, *53*, 1416–1428.
12. Zhou, X.; Wang, S.; Li, X.; Meng, J.; Li, Z.; Zhang, L.; Pu, D.; Wang, L. Research on Theory and Technology of Floor Heave Control in Semicoal Rock Roadway: Taking Longhu Coal Mine in Qitaihe Mining Area as an Example. *Lithosphere* **2022**, *2022*, 3810988. [CrossRef]
13. Krishna, P.H.; Murty, V.R. Long-term Field Heave Studies on Various Foundation Techniques in Expansive Soils. *Indian Geotech. J.* **2021**, *51*, 909–923. [CrossRef]
14. Zhao, J.; Duan, S.; Chen, B.; Li, L.; He, B.; Li, P.; Liu, G. Failure mechanism of rock masses with complex geological conditions in a large underground cavern: A case study. *Soil Dyn. Earthq. Eng.* **2024**, *177*, 108439.
15. Xu, C.; Zhang, W. Risk Analysis of Slope Edge Uplift of Coal Mining Area Based on New Response Surface Method. *J. Wuhan Univ. Technol.* **2017**, *39*, 56–61.
16. Zhang, Z.T.; Gao, W.H.; Wang, X.; Zhang, J.Q.; Tang, X.Y. Degradation-induced evolution of particle roundness and its effect on the shear behaviour of railway ballast. *Transp. Geotech.* **2020**, *24*, 100388. [CrossRef]
17. Savvides, A.A.; Papadrakakis, M. A computational study on the uncertainty quantification of failure of clays with a modified Cam-Clay yield criterion. *SN Appl. Sci.* **2021**, *3*, 659. [CrossRef]
18. Chwala, M. Undrained bearing capacity of spatially random soil for rectangular footings. *Soils Found.* **2019**, *59*, 1508–1521. [CrossRef]
19. Yan, C.; Xu, J.; Bao, H. *Rock Mass Mechanics*; Beijing People's Communications Press: Beijing, China, 2017; pp. 123–125.
20. Zhang, Z.; Liu, H. A Special Case of History the Environmental Impact by Underground Mining-The Mechanism and Measure of the Ground Upheaval Deformation of Hancheng Power Plant. *Earth Sci. Front.* **2001**, *8*, 285–295.